

Chieh Lin  
Alain Luciani  
Emmanuel Itti  
Taoufik El-Gnaoui  
Alexandre Vignaud  
Pauline Beaussart  
Shih-ju Lin  
Karim Belhadj  
Pierre Brugières  
Eva Evangelista  
Corinne Haioun  
Michel Meignan  
Alain Rahmouni

## Whole-body diffusion-weighted magnetic resonance imaging with apparent diffusion coefficient mapping for staging patients with diffuse large B-cell lymphoma

Received: 18 November 2009  
Revised: 1 February 2010  
Accepted: 7 February 2010  
Published online: 23 March 2010  
© European Society of Radiology 2010

C. Lin · A. Luciani · P. Beaussart ·  
P. Brugières · A. Rahmouni (✉)  
Imagerie Médicale, AP-HP,  
Groupe Henri-Mondor Albert-  
Chenevier, CHU Henri Mondor,  
51 Avenue du Malréchal de  
Lattre de Tassigny,  
94010 Créteil, France  
e-mail: alain.rahmouni@hmn.aphp.fr  
Tel.: +33-1-49812631  
Fax: +33-1-49812632

C. Lin · A. Luciani · E. Itti ·  
P. Beaussart · P. Brugières · C. Haioun ·  
M. Meignan · A. Rahmouni  
Université Paris-Est Créteil Val de  
Marne, Faculté de Médecine,  
94010 Créteil, France

E. Itti · M. Meignan  
CNRS, UMR7054,  
94010 Créteil, France

A. Luciani  
INSERM Unité U955,  
Equipe 17,  
94010 Créteil, France

E. Itti · E. Evangelista · M. Meignan  
Médecine Nucléaire, AP-HP,  
Groupe Henri-Mondor Albert-  
Chenevier, CHU Henri Mondor,  
51 Avenue du Malréchal de  
Lattre de Tassigny,  
94010 Créteil, France

T. El-Gnaoui · K. Belhadj · C. Haioun  
Hématologie Clinique, AP-HP,  
Groupe Henri-Mondor Albert-  
Chenevier, CHU Henri Mondor,  
51 Avenue du Malréchal de  
Lattre de Tassigny,  
94010 Créteil, France

A. Vignaud  
Siemens Healthcare,  
9 Boulevard Finot,  
93527 Saint-Denis, France

S.-j. Lin  
Department of Statistics,  
Stanford University,  
450 Serra Mall,  
Stanford, CA 94305, USA

**Abstract Objective:** To design a whole-body MR protocol using exclusively diffusion-weighted imaging (DWI) with respiratory gating and to assess its value for lesion detection and staging in patients with diffuse large B-cell lymphoma (DLBCL), with integrated FDG PET/CT as the reference standard. **Methods:** Fifteen patients underwent both whole-body DWI ( $b=50, 400, 800 \text{ s/mm}^2$ ) and

PET/CT for pretreatment staging. Lymph node and organ involvement were evaluated by qualitative and quantitative image analysis, including measurement of the mean apparent diffusion coefficient (ADC).

**Results:** A total of 296 lymph node regions in the 15 patients were analysed. Based on International Working Group size criteria alone, DWI findings matched PET/CT findings in 277 regions (94%) (kappa score=0.85,  $P<0.0001$ ), yielding sensitivity and specificity for DWI lymph node involvement detection of 90% and 94%. Combining visual ADC analysis with size measurement increased DWI specificity to 100% with 81% sensitivity. For organ involvement, the two techniques agreed in all 20 recorded organs (100%). All involved organ lesions showed restricted diffusion. Ann Arbor stages agreed in 14 (93%) of the 15 patients.

**Conclusion:** Whole-body DWI with ADC analysis can potentially be used for lesion detection and staging in patients with DLBCL.

**Keywords** Diffusion-weighted imaging · ADC mapping · Respiratory gating · Diffuse large B-cell lymphoma · Staging · FDG PET/CT

### Introduction

Determination of disease extent is essential for appropriate treatment planning and prognostication in patients with

malignant lymphoma. Contrast-enhanced computed tomography (CECT) is currently the imaging technique most commonly used for staging and follow-up, with International Working Group (IWG) criteria [1, 2]. Positron

emission tomography (PET) with fluorine 18-fluorodeoxyglucose (FDG) or, more recently, coregistered FDG PET/CT performed with non-enhanced CT has been shown to be more accurate than CECT for evaluation of disease extent [3–5] and treatment response [6, 7] by providing metabolic information in patients with aggressive lymphoma. In addition, the standardised uptake value (SUV), a semi-quantitative index, is helpful for determining disease aggressiveness, for objective treatment response assessment and for outcome prediction [8–11].

Diffusion-weighted magnetic resonance imaging (DWI) probes noninvasively random microscopic motion of water molecules in the body. Because of their high cellularity and high nuclear-to-cytoplasm ratio, aggressive lymphomas such as diffuse large B-cell lymphoma (DLBCL) have relatively high signal intensity on diffusion-weighted (DW) images [12]. In addition, lymphomas have lower apparent diffusion coefficients (ADC) than other tumour types in different body regions [12–15]. The development of ultrafast imaging sequences, high-gradient amplitudes, multichannel coils and parallel imaging have led to increasing use of DWI for the evaluation of extracranial diseases, including on the whole-body scale [16–20]. Several studies have shown the potential of whole-body DWI for lymphoma staging [21–24], but they included patients with other types of malignancies or both Hodgkin or non-Hodgkin lymphoma patients with different histological grades.

Thus, the aims of this pilot study focusing on patients with DLBCL were (1) to design a whole-body MR protocol using exclusively DWI with respiratory gating suitable for routine imaging and (2) to assess its value with and without ADC analysis for lesion detection and staging, with integrated FDG PET/CT as the standard of reference.

## Materials and methods

### Patients

This prospective study was approved by our institutional review board, and all the patients gave their written informed consent. The following patients were eligible: adults with histologically proven DLBCL requiring pre-treatment staging. The exclusion criteria were patients with other malignancies or haematological disorders and contraindications to MRI, such as claustrophobia and implanted pacemakers. Between June 2008 and February 2009, 15 patients who met the inclusion criteria underwent both whole-body DWI and integrated FDG PET/CT within an average of 3 days (range, 1–8 days) of each other. Pathological diagnosis was established by lymph node biopsy (n=13), tonsillectomy (n=1) or splenectomy (n=1). Imaging studies were performed within 2 weeks following the histological diagnosis, and no treatment was given during this period. Staging was based on the Ann Arbor system, with physical examination, CECT, integrated FDG

PET/CT and bone marrow biopsy, all practiced at our institution [2, 25, 26]. Characteristics of the study population are shown in Table 1.

### Whole-body DWI protocol design

All examinations were performed on a 1.5-T MR system (Magnetom Avanto equipped with Syngo MR B15 software; Siemens Healthcare, Erlangen, Germany) with high-gradient performance (amplitude, 40 mT/m; slew rate, 170 [mT·m<sup>-1</sup>]/ms). The MR scanner was equipped with a total imaging matrix (TIM) system, which enables one to connect up to 76 surface coil elements and to use up to 18 of them for a given field of view (FOV). The patients were positioned supine and head-first in the magnet bore, with five sets of phased-array surface coils installed simultaneously to cover the head, neck, chest and abdomen, and the pelvis to the upper thighs; the spine coils were embedded in the patient table.

Our whole-body DW MR protocol consisted exclusively of a single-shot spin-echo echo-planar technique (SS SE-EPI) with spectrally selective fat saturation. Although short-tau inversion recovery (STIR) theoretically gives more homogeneous fat saturation because of its insensitivity to magnetic field heterogeneity, the image acquisition time is twice as long and the signal-to-noise ratio is lower

**Table 1** Patient characteristics

Variable	Value
No. of men/women	9/6
Mean age of entire population (years)	48 (23–79)
Histology	
DLBCL	13
Concomitant DLBCL and follicular lymphoma	2
Disease status	
First-line/relapse	13/2
Standard IPI score	
0–2 (low risk)	9
3–5 (high risk)	6
Ann Arbor Stage	
I-II	3
III-IV	12

Data are the number of patients. Data in parentheses are the range. DLBCL = diffuse large B-cell lymphoma. The median age of the entire population was 51 years

Two patients presented with concomitant DLBCL and follicular lymphoma, both proven histologically

The International Prognostic Index (IPI) is based on age, tumour stage, the serum lactate dehydrogenase concentration, performance status and the number of extranodal disease sites [45]. The Ann Arbor stage is based on physical examination, contrast-enhanced CT, integrated FDG PET/CT and bone marrow biopsy

[19]. All DW images were acquired in the transverse plane. For ADC mapping, slice position mismatch between different b values and different excitations must be minimised [19, 27]. Therefore, a respiratory-gated acquisition was preferred to free breathing [16, 19, 24]. All DW images were acquired using an air-filled pressure sensor fixed to the hypochondrial region with a belt, which is the only method of ensuring a gating in regions outside the diaphragm in comparison to a navigator-triggered technique. Three trace b values, 50, 400 and 800 s/mm<sup>2</sup> (b50, b400 and b800; instead of the commonly used two data points), were used to improve the accuracy of ADC calculation [14] and to maintain a reasonable acquisition time. The DW gradients were applied orthogonally in the slice-selective (superoinferior), phase-encoding (anteroposterior) and read-out (right-to-left) directions, with four signals acquired, a partial Fourier factor of 7/8, a bandwidth of 1,602 Hz/pixel, a 130×108 matrix, a 330–400-mm FOV adapted to the patient's habitus and a rectangular FOV of 83.1% (voxel size≈3×3×5 mm<sup>3</sup>). ADC maps were automatically generated from DW images by the MR software. The lowest b value of 50 s/mm<sup>2</sup> (instead of 0) was chosen to eliminate signals from vessels and also to reduce perfusion effects [18, 28]. In addition, images obtained with a b value of 50 s/mm<sup>2</sup> can serve as T2-weighted images, thus providing anatomical information. The highest b value was set at 800 s/mm<sup>2</sup> in order to enhance the lesion-to-normal tissue conspicuity [19] but to avoid excessive image distortion and signal loss [14, 29].

The repetition time (TR) was equal to the duration of a respiratory cycle (≈3,000 ms). Images were acquired during each expiration plateau, with a constant acquisition window of 1,800 ms (Fig. 1). The patients were instructed to breath regularly during the entire examination.

Parallel imaging (generalised autocalibrating partially parallel acquisition: GRAPPA) and a parallel acceleration factor of 2 were used in order to shorten the echo time (TE), which was set at 73 ms, the shortest value allowed by the system with the chosen parameters, to minimise image distortion due to magnetic susceptibility. Good fat saturation was also needed to avoid chemical shift artefacts, which appear in the phase-encoding direction in EPI [30]. For both purposes, the centre of each stack of images (i.e. each station) was placed in the most homogeneous region of the magnet (i.e. the isocentre) during acquisition, and a B0 shim was performed systematically for each station. In addition, to improve the shim convergence, each station was limited to 28 slices with a slice thickness of 5 mm (i.e. 14 cm in height). In order to avoid possible crosstalk [30], each station was completed with the acquisition of two sets of images: each of 14 slices with a 5-mm interslice gap [31] and shifted by 5 mm, enabling contiguous images. Six to seven stations of 28 images were required to span the skull base to the groin region. The acquisition time of each station was about 6 min. The total acquisition time, which depended on the patient's height and respiratory rate, ranged from 30 to 45 min.

## Integrated FDG PET/CT

PET/CT examinations were performed with a 16-detector PET/CT system (Gemini GXL, Philips Medical Systems, DA Best, The Netherlands). Patients fasted for at least 6 h before imaging, which started about 60 min after the injection of 5 MBq/kg FDG. No intravenous or oral contrast agents were administered. The acquisition consisted of low-dose transmission CT (100 kV, 80 mAs, slice thickness 5 mm), followed by the emission imaging in 9–11 overlapping bed shifts to cover the skull vault to mid-thigh, each with an 18-cm FOV and lasting 2 min. Images (144×144 matrix, voxel size 4×4×4 mm<sup>3</sup>) were reconstructed with a line-of-response reconstruction algorithm. SUV was normalised to body weight and calculated as described elsewhere [11].

## DWI image analysis

Axial DW images were prospectively interpreted by two radiologists, one with 7 years' and the other with 20 years' experience in body MR imaging, who were unaware of all clinical, CECT and PET/CT findings, except for the patient's diagnosis. Lesion detection and size measurement were performed on b50 DW images. However, b400 and b800 images were also carefully examined in order not to overlook organ involvement that could be masked by surrounding normal tissue (kidney, for example) with a T2 shine-through effect. The two readers reached a consensus on whether a lymph node region or an organ was involved (i.e. positive or negative). The following 20 regions were used for anatomical assignment of lymph node involvement: Waldeyer's ring, right and left cervical, right and left axillary, right and left internal mammary/diaphragmatic, anterior mediastinal, paratracheal, right and left hilar, subcarinal/posterior mediastinal, coeliac/superior mesenteric, hepatic and splenic hilar, retroperitoneal, inferior mesenteric, right and left iliac, and right and left inguinal regions. Organ involvement was assessed in the lungs, liver, spleen, kidneys, gastrointestinal tract and bone marrow. Lymphoma involvement elsewhere was also noted.

## Lymph node involvement

- Size criteria

In keeping with IWG criteria [1], a lymph node that was larger than 10 mm in its longest transverse diameter was considered positive for lymphoma involvement, except for those with a clearly identified fatty hilum and thin cortex.

- Visual ADC analysis

For each lymph node region recorded positive for lymphoma involvement based on IWG size criteria, the

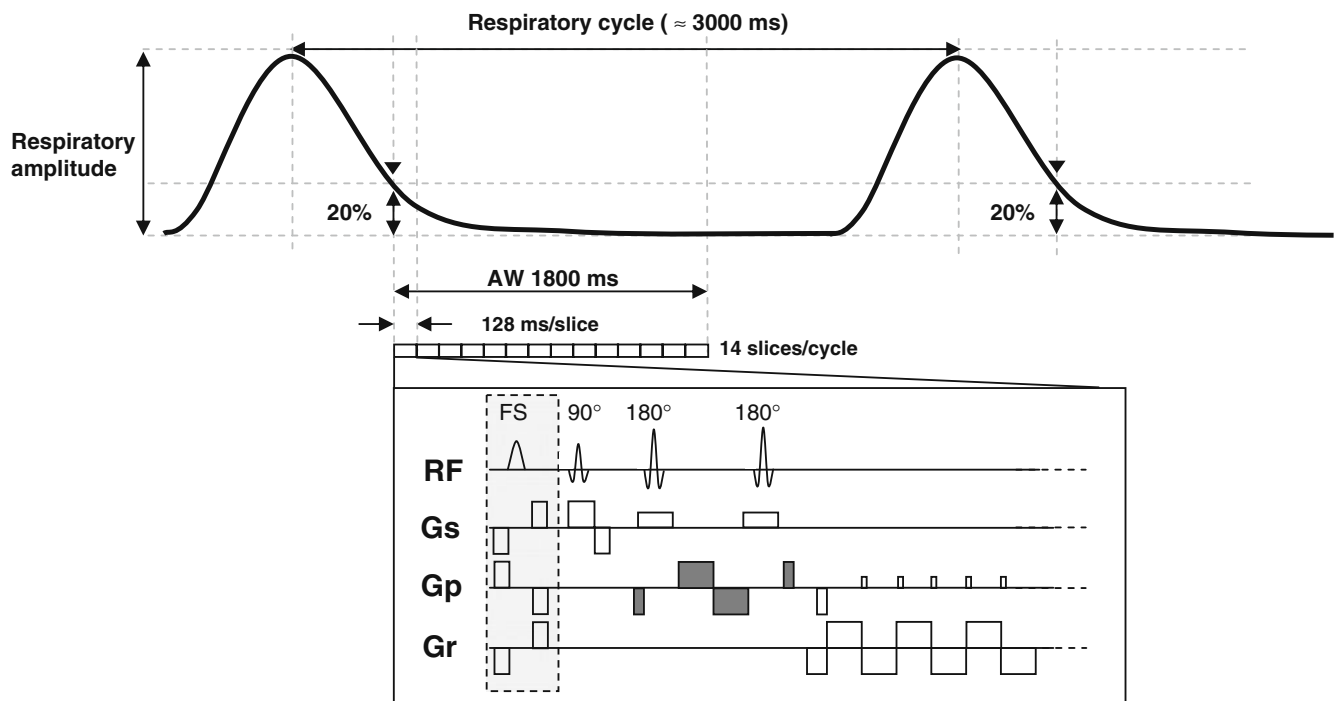


**Fig. 1** Schematic illustration of the respiratory-triggered single-shot spin-echo echo-planar sequence (SS SE-EPI) used in our study. The sequence is built around a twice-refocused spin echo optimised to reduce eddy-current-induced image distortion [44]. Fourteen slices were acquired during each expiration plateau with a constant

acquisition window (AW) set at 1,800 ms. RF = radiofrequency pulse, Gs = slice-selection gradient, Gp = phase-selection gradient, Gr = readout-selection gradient, FS = fat saturation. In this example, the diffusion gradients (grey boxes) were applied to the phase-encoding direction

lesion signal intensity on ADC maps was visually assessed as either iso- to hyperintense or hypointense to muscle on the same image slice. Masses with both hyper- and hypointense areas were recorded as hypointense to muscle. A signal hypointense to muscle indicated restricted diffusion.

#### *Organ involvement*

Organ involvement was considered present when any signal abnormality or mass lesion was identified, excluding simple cysts (i.e. frank signal loss on b800 images with cerebrospinal fluid (CSF)-like signal on ADC maps). Splenomegaly (longest diameter > 13 cm) without focal lesions and without MR signs of liver cirrhosis was considered positive.

Visual ADC analysis was also performed for each organ recorded positive for lymphoma involvement based on signal abnormality criteria.

#### *ADC measurement*

One author performed region-of-interest (ROI) measurement with an off-line Mac OS workstation (MacBook, Apple Computer, Cupertino, CA) and dedicated image processing software (OsiriX version 3.3.2, Los Angeles,

CA). For each lymph node region and organ recorded as positive on DWI, the lesion showing the lowest signal intensity on ADC maps was identified. DW images with b values of 50, 400 and 800 s/mm<sup>2</sup> were carefully examined to ensure that no motion had occurred among the three trace images. ROI measurement was then done directly on the parametric ADC maps. On the single slice with lowest signal intensity assessed by visual analysis, an ROI was manually drawn to encompass the entire cross section of the lesion. Any necrotic areas, i.e. areas of high signal intensity close to that of CSF on b50 images were excluded [14]. The mean ADC (ADC<sub>mean</sub>) within this ROI was recorded. In one patient, who had splenomegaly without focal lesions, a circular ROI was drawn on the spleen.

The ADC<sub>mean</sub> of the upper thoracic spinal cord was also measured on a single slice with a manually drawn ROI encompassing its entire cross section, in order to be used as a control value [14, 29, 32].

#### *Integrated FDG PET/CT image analysis*

Axial images as well as multiplanar reformats (MPR) and maximal intensity projection (MIP) ones were prospectively interpreted by one nuclear medicine physician with 9 years' experience in reading PET, who was unaware of clinical, CECT and MR data, except for the patient's



diagnosis. After upper-thresholding the data in order to place liver activity at around 30% on the grey scale [10, 11], any focus of increased FDG uptake (over background) not located in areas of physiologically increased uptake was considered to indicate lymphoma involvement, whatever its size [2]. Lymph node and organ involvement were recorded for the same anatomical regions as those used for DWI. Organ involvement was considered present when focal or heterogeneous uptake was seen [2]. Homogeneously increased FDG uptake by the spleen, higher than that of the liver, was also considered positive [33, 34].

#### SUV measurement

The same author who performed ADC measurement performed ROI measurement on a Gemini workstation with software (Syntegra version 2.1J, Milpitas, CA). For each lymph node region and organ recorded as positive on integrated PET/CT, the lesion with the highest FDG uptake was identified. An ROI encompassing the entire cross-section of the lesion was manually drawn on the single axial slice of the PET image containing the pixel with the maximum standardised uptake value (SUVmax). The SUVmax value was recorded to indicate the glycolytic activity of the lesion [10]. In one patient, who had splenomegaly showing homogeneously increased FDG uptake higher than that of the liver, a circular ROI was drawn on the spleen.

#### Statistical analysis

Data were analysed on a per-lymph node region or a per-organ basis. Qualitative variables are reported as percentages and quantitative variables as means  $\pm$  standard deviation. Kappa coefficients were calculated to evaluate agreement between the two imaging techniques for lymph node involvement. Agreement was considered poor at a  $\kappa$  value of 0; weak at 0.01–0.20; fair at 0.21–0.40; moderate at 0.41–0.60; good at 0.61–0.80; excellent at 0.81–1 [35].

Sensitivity and specificity of DWI for lymphoma involvement were evaluated with PET/CT as the reference standard, first with (1) size (lymph node) or signal abnormality (organ) criteria alone, and second with (2) combined size and visual ADC analysis, i.e. lymph node larger than 10 mm in its longest transverse diameter with restricted diffusion on ADC maps and/or organ involvement with restricted diffusion on ADC maps, being considered “positive” for lymphoma involvement. The mean ADCmean of lymph node regions positive on both DWI (size criteria) and PET/CT was compared with that of the spinal cord in each patient with a two-tailed paired t test. P values <0.05 were assumed to indicate significant

differences. The impact of DWI and PET/CT on disease staging was analysed according to Ann Arbor staging as defined in the patient section. The Prism 5.0 software package for Windows (GraphPad Software, La Jolla, CA) and the R statistical software package (R Development Core Team, Vienna, Austria) were used for statistical analyses.

## Results

All 300 lymph node regions (20 regions per patient) were successfully evaluated by PET/CT. DW images of six lymph node regions covering the upper chest could not be analysed in one patient because of technical failure and were therefore excluded from further analysis. Among these six regions, PET/CT identified two regions with lymphoma involvement. In two patients, both DWI and PET/CT showed another lymph node region (left femoral region in one patient and presacral region in the other patient) in addition to the above-mentioned regions. Therefore, a total of 296 lymph node regions were available for analysis on both imaging techniques. No movement was detected among the three trace DW images when performing ROI selection in all 15 patients.

#### Lymph node involvement

The results of DWI based on size (longest transverse diameter >10 mm) alone or on combined size and visual ADC analysis are compared with PET/CT findings in Table 2.

Based on size criteria alone, DW and PET/CT results matched in 277 regions (94%). The agreement between two imaging techniques was excellent ( $\kappa=0.85$ ,  $P<0.0001$ ). The sensitivity and specificity of DWI for lymph node involvement on a per-region basis was 90% (82/91) and 94% (195/205).

With combined size and visual ADC analysis, DW and PET/CT results still agreed in 277 regions with excellent agreement ( $\kappa=0.84$ ,  $P<0.0001$ ). The sensitivity decreased to 81% (73/91) but the specificity increased to near 100% (204/205) (Table 2). The single false-positive region detected on DWI was in a patient with perigastric lymph node involvement, which was masked by FDG uptake of the primary gastric mass and thereby considered negative on PET/CT. This finding was confirmed on CECT. Therefore, the positive predictive value reached 100% with this combined approach.

Among the 82 lymph node regions that were positive on both DWI (size criteria alone) and PET/CT, the lymph nodes were visually hypointense to muscle on ADC maps (restricted diffusion) in 73 regions (89%) (Fig. 2). The mean ADCmean of the 73 regions showing restricted diffusion was  $0.752 \times 10^{-3} \text{ mm}^2/\text{s} \pm 0.210$  (range 0.431–

**Table 2** Per-region comparison of lymph node involvement on whole-body DWI and integrated FDG PET/CT

	PET/CT		PET/CT	
	Positive	Negative	Positive	Negative
DWI criteria	Size alone		Size plus visual ADC analysis	
Positive	82	10	73	1
Negative	9	195	18	204

Data are the number(s) of lymph node regions. DWI = diffusion-weighted magnetic resonance imaging, FDG = fluorodeoxyglucose, PET = positron emission tomography, CT = computed tomography. ADC = apparent diffusion coefficient

DWI interpretation criteria: size criteria alone: a lymph node that was larger than 10 mm in its longest transverse diameter was considered positive for lymphoma involvement [1]; size plus visual ADC analysis: a lymph node larger than 10 mm with restricted diffusion (i.e. hypointense to muscle on ADC maps) was considered positive for lymphoma involvement

1.403), and the mean SUVmax was  $9.8 \pm 7.6$  (range 1.5–26.3). The mean ADCmean of the nine regions showing no restricted diffusion (iso- to hyperintense to muscle) was  $1.563 \times 10^{-3} \text{ mm}^2/\text{s} \pm 0.455$  (range 1.074–2.523), and the mean SUVmax was  $4.5 \pm 3.1$  (range 2.0–11.7). In three of these nine regions, PET/CT depicted node involvement over the pericardiac region (left internal mammary/diaphragmatic chain) in three patients, with a mean SUVmax of 7.7 (range 5.3–11.7). These lymph nodes were also positive on DWI, based on size criteria. However, they were all hyperintense to muscle on ADC maps, with a mean ADCmean of  $1.920 \times 10^{-3} \text{ mm}^2/\text{s}$  (range 1.521–2.523).

In seven patients, DWI depicted additional lymph node involvement in 10 regions (3 cervical/1 axillary/2 hilar/1 internal mammary/1 coeliac and superior mesenteric/2 inguinal) based on size criteria, but without abnormal FDG uptake. None of these lymph nodes, except for the above-mentioned perigastric lymph node involvement (ADCmean  $0.681 \times 10^{-3} \text{ mm}^2/\text{s}$ ), showed restricted diffusion on ADC maps. The mean ADCmean of the remaining nine regions was  $1.520 \times 10^{-3} \text{ mm}^2/\text{s}$  (range 1.228–2.137).

In six patients, PET/CT depicted additional lymph node involvement in nine regions, with a mean SUVmax of 2.6 (range 1.4–4.5). The involvement in five of these nine regions was not detected on DW images, owing to incomplete fat saturation ( $n=4$ , cervical and anterior mediastinal regions) or to unknown causes ( $n=1$ , subcarinal region). The other four regions were not considered positive on DW images, owing to their small size ( $n=3$ , longest diameter  $\leq 10$  mm) or because the nodes had a thin cortex and fatty hilum ( $n=1$ ). It should be noted that in one patient, a 7-mm left cervical lymph node (SUVmax 3.8), with adequate fat saturation, was also identified on DW images and showed restricted diffusion on ADC maps, with an ADCmean of  $0.929 \times 10^{-3} \text{ mm}^2/\text{s}$  (Fig. 3).

The ADCmean of the upper thoracic spinal cord in the 15 patients averaged  $1.039 \times 10^{-3} \text{ mm}^2/\text{s} \pm 0.061$  (range

$0.929$ – $1.139$ ). In 14 patients with lymph node regions positive on both DWI (size criteria) and PET/CT, the mean ADCmean of lymph nodes was significantly lower than that of the spinal cord (paired t test,  $P=0.03$ ).

#### Organ involvement

In 12 of the 15 patients, extranodal disease was detected on both DWI and PET/CT. In total, 20 organs were found to be involved. The two imaging techniques agreed on 20. The sensitivity and specificity of DWI based on signal abnormality alone were 100%. Table 3 summarises the involved organs and the number of patients. Two patients had liver involvement: one had multiple nodules (Fig. 2), which were clearly identified on both techniques; the other patient had a heterogeneous signal abnormality of the liver and numerous focal lesions on DW images, while PET identified only two faint focal increases in FDG uptake, with no discernible lesions on CT (Fig. 4). Among the three patients with spleen involvement, one patient had diffuse involvement on PET/CT and splenomegaly on DWI, another patient had multifocal lesions depicted on both techniques, and the third patient had both diffuse and focal spleen involvement while DWI depicted only focal lesions (Fig. 2). Bone marrow involvement was noted in five patients (Fig. 5).

The lesions showed restricted diffusion on ADC maps in all 20 (100%) organs. The mean ADCmean was  $0.680 \times 10^{-3} \text{ mm}^2/\text{s} \pm 0.148$  (range 0.448–0.921), and the mean SUVmax was  $14.0 \pm 9.5$  (range 3.1–37.8). The sensitivity and specificity remained unchanged when the results of visual ADC analysis were taken into account.

#### Ann Arbor stages

Finally, Ann Arbor stages based on DWI without ADC analysis and those of PET/CT agreed in 14 patients (93%), two of whom had stage II, one stage III and 11 stage IV

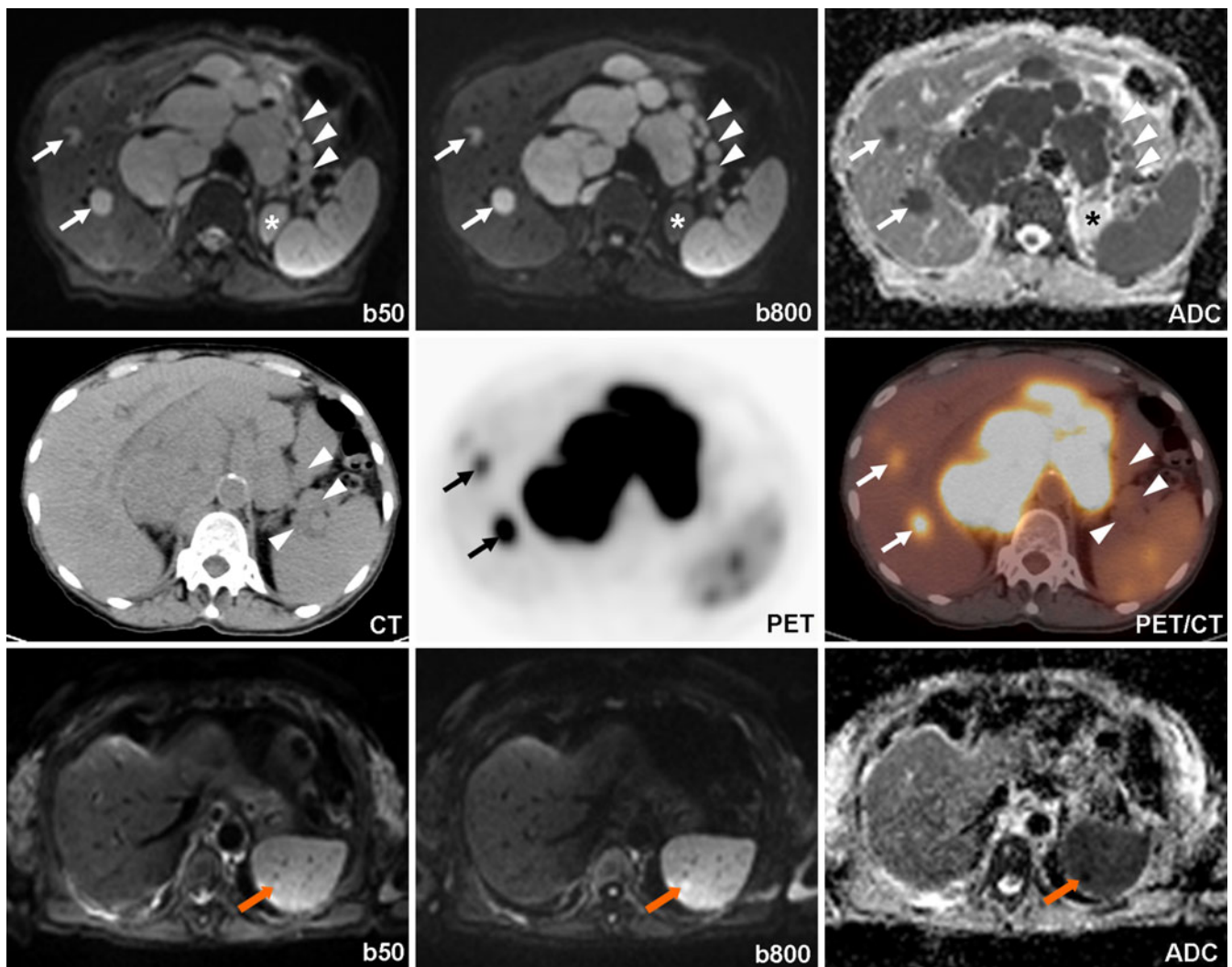


**Fig. 2** Concordant detection of coeliac and retroperitoneal lymph node involvement by DWI with  $b$  values of 50 and  $800 \text{ s/mm}^2$  ( $b50$  and  $b800$ ) and their corresponding apparent diffusion coefficient (ADC) map (upper row) and integrated FDG PET/CT (middle row) in a 79-year-old patient with concomitant diffuse large B-cell lymphoma and follicular lymphoma. The slice levels are slightly different using the two imaging techniques. These lymph nodes all show restricted diffusion on the ADC map and intense FDG uptake on PET, consistent with large cell lymphoma. Note that the signal intensity of the normal left kidney (\*) drops on the  $b800$  DW image, which shows no restricted diffusion on the ADC map. However,

multiple superior mesenteric and splenic hilar lymph nodes (arrowheads), also with restricted diffusion on the ADC map, showed very faint FDG uptake (probably due to a follicular component). Multinodular hepatic involvement (arrows in white/black) was detected with both techniques. Both diffuse (higher FDG uptake than liver) and focal splenic involvement were depicted on PET/CT. As normal spleen already shows restricted diffusion on DW images, only four focal lesions (each  $< 10 \text{ mm}$ ) with even more restricted diffusion were depicted on DWI (lower row, orange arrow, example of an 8-mm nodule). Note also that water diffusion in normal bone marrow is restricted

disease. Stages of these 14 patients also agreed with the combined techniques, including physical examination, CECT, PET/CT and bone marrow biopsy. With combined ADC analysis, Ann Arbor stages of these 14 patients remained unchanged.

The remaining patient had stage III disease based on DWI and stage I based on PET/CT. On PET/CT, the perigastric nodes were masked by FDG uptake of the

gastric tumour (downstage to one localised extranodal disease: stage I). In addition to gastric and perigastric lymph node involvement, DWI depicted an additional 15-mm node over the left cervical region (upstage to stage III). However, this lymph node was isointense to muscle on ADC maps, with an  $\text{ADC}_{\text{mean}}$  of  $1.175 \times 10^{-3} \text{ mm}^2/\text{s}$ . Stage II disease was assigned based on the combined techniques.

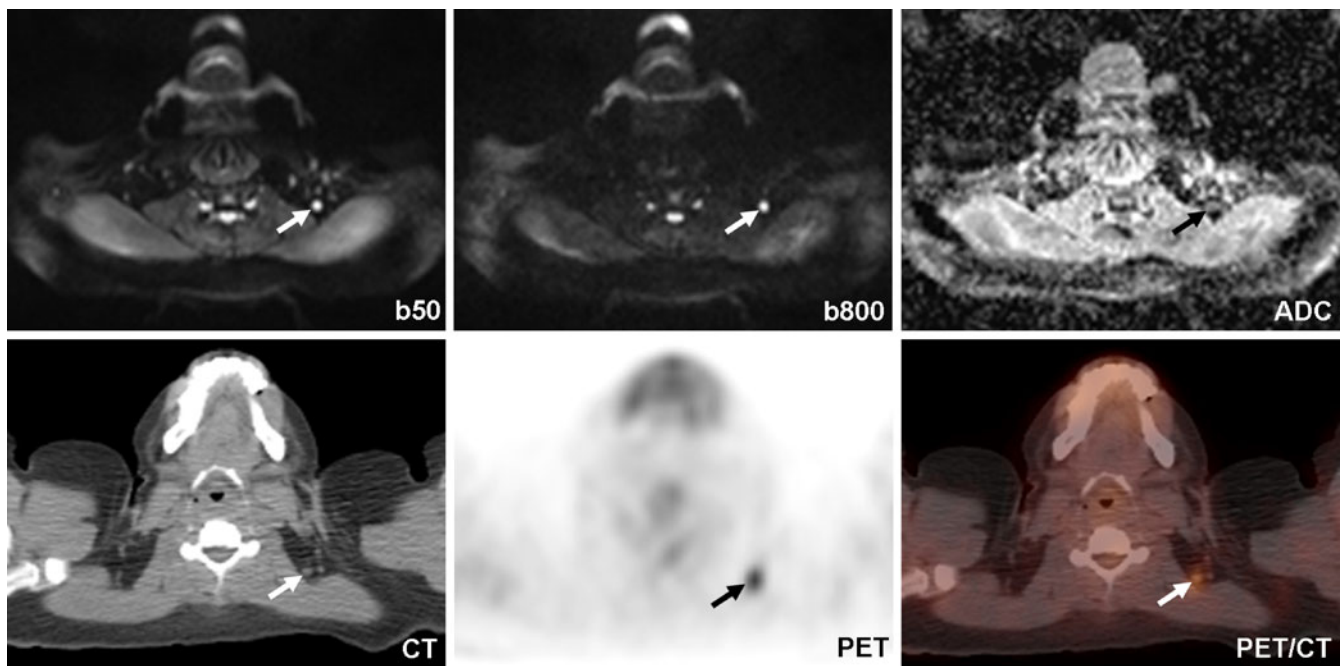


**Fig. 3** Left cervical subcentimetric lymph node involvement in a 60-year-old patient with diffuse large B-cell lymphoma. A 7-mm round lymph node (arrow) was depicted on PET/CT with abnormal

FDG uptake (lower row). This lymph node was considered negative on DWI (upper row) based on size criteria, but was clearly identified on the basis of restricted diffusion

## Discussion

This pilot study shows that a whole-body MR protocol using exclusively DWI with respiratory gating can be used to stage patients with DLBCL. Our preliminary results show excellent agreement between DWI and PET/CT regarding both lymph node and organ involvement. DWI, which reflects tissue structure and cellularity, might be complementary to FDG-PET, which indicates glucose metabolic activity and disease aggressiveness [36, 37]. Several studies have demonstrated the potential of whole-body DWI for lesion detection in oncology patients [16, 19,

21–23, 38]. A recent whole-body DWI study including lymphoma patients with comparison to CECT showed that initial staging using whole-body MRI with T1-, T2-weighted images and DWI equals staging using CECT in most patients and correctly overstaged in 6 (21%) out of 28 patients relative to CECT [24]. However, these authors did not assess the usefulness of whole-body DWI alone for lymphoma staging.

Our study with comparison to integrated FDG PET/CT also shows that size-based analysis of lymph node involvement in DLBCL may be supplemented by the information provided by whole-body ADC mapping. In the only patient who was assigned different Ann Arbor stages by DWI and PET/CT, in addition to subdiaphragmatic disease, DWI depicted an additional enlarged lymph node (longest transverse diameter 15 mm) over the left cervical region. However, this node did not show restricted diffusion on ADC maps. Conversely, lymph nodes in 89% of the 82 concordantly positive regions based on DWI size criteria showed restricted diffusion on ADC maps. Therefore, with combined ADC analysis, this lymph node might have been considered negative, and the patient would have been correctly staged. For lymph node involvement, combined size and visual ADC analysis criteria led to near 100% specificity, but at the expense of decreased sensitivity. Some PET-positive lymph node regions that showed high ADC values had low SUV values. In addition, small PET-positive lymph nodes that showed high ADC values were located in regions adjacent

**Table 3** Organ involvement

Organ	Number of patients
Lungs	1
Liver	2
Spleen	3
Kidneys	2
Gastrointestinal tract (stomach)	1
Bone marrow	5
Others	
Breast	1
Adrenal glands	1
Skin/subcutis/muscles	4



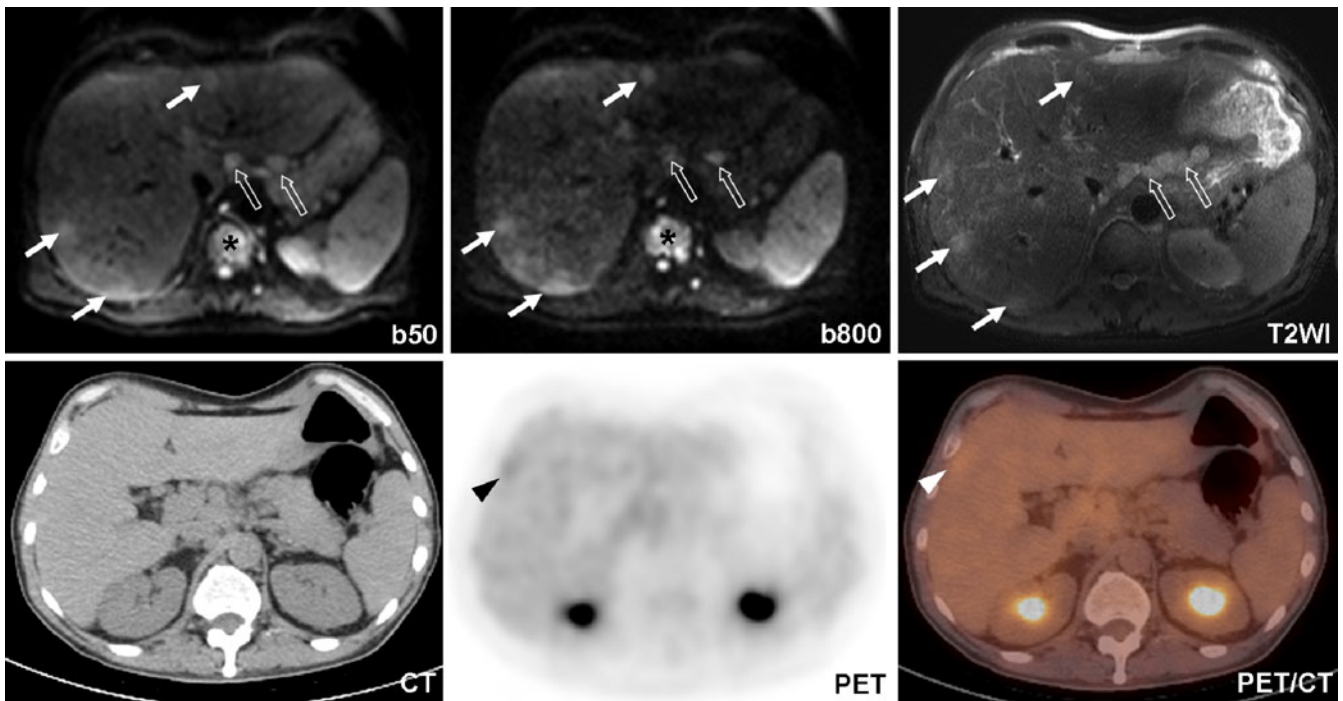


**Fig. 4** Liver involvement in a 57-year-old patient with concomitant diffuse large B-cell lymphoma and follicular lymphoma. Liver signal intensity was heterogeneous, and multiple focal hepatic lesions (arrows) were detected on *b50* and *b800* DW images (upper row). Hepatic involvement was confirmed 4 days later on a dedicated hepatic T2-weighted MR image (T2WI) (similar slice

level). Note also the coeliac lymph node (open arrows) and bone marrow involvement (\*). PET/CT images at this slice level showed no abnormal FDG uptake (images not shown). At a lower slice level, PET/CT (lower row) revealed a focus of faintly increased FDG uptake (arrowhead), but no lesion was discernible on the co-registered CT image

to lungs or heart. In these patients, we cannot exclude the possibility that susceptibility artefacts at the air-tissue interface or heart motion could have resulted in falsely high ADC values [24].

Whole-body DWI is generally performed with free breathing [16, 19, 24]. It has been more extensively studied in the liver, and there is still debate regarding the reproducibility of ADC measurement with respiratory gating over the other respiratory schemes, namely breath-hold or free breathing [39]. Whole-body DWI with continuous breathhold acquisition is clinically not feasible. While ADC measurement of a large, nearly uniform structure such as the liver appears to be accurate with free breathing, respiratory motion can still result in ADC errors for small focal lesions such as lymph nodes because of signal contamination by adjacent tissues [19, 27]. Therefore, although the acquisition time is longer than with free breathing, we chose to use respiratory gating in order to achieve better accuracy in our ADC measurements. Our ADCmean values for the spinal cord were similar to those published elsewhere [14, 40].

Whole-body DWI is generally performed with STIR fat saturation [16, 19, 24]. Instead of STIR, we chose spectrally selective fat saturation in order to increase the signal-to-noise ratio and to reduce the acquisition time.

Regarding the limitations of our study, our group of 15 patients may be too small to be representative of the DLBCL patient population. However, all 15 patients had a pathological diagnosis of DLBCL. Pathological proof of each lesion detected by DWI was neither possible nor ethical, and we therefore used integrated FDG PET/CT as the reference standard [3–5]. Furthermore, one patient had an 8-day interval between the two imaging examinations, but no treatment was given during this period, as in the other 14 cases. Our DWI was not a real whole-body protocol, but spanned only the skull base to the groin. Anatomical coverage was similar to that of the CECT. Another limitation is our choice of  $50 \text{ s/mm}^2$  as the lowest *b* value, as it might result in residual perfusion effects on our ADC values. However, most perfusion effects are eliminated with a *b* value of  $50 \text{ s/mm}^2$  [18] compared with the commonly used  $0 \text{ s/mm}^2$ . Furthermore, *b50* DW images eliminated signals from vessels [28] and maintained good T2 contrast (our protocol did not include conventional MR sequences). The ROIs in our study were not volumetric, but this did not have an impact on SUV values as only the maximum value was used. Conversely, ADCmean values were recorded as the single-pixel minimum ADC value might have been subject to signal fluctuation or to misregistration of the trace images. Therefore, ADCmean values might not have represented the

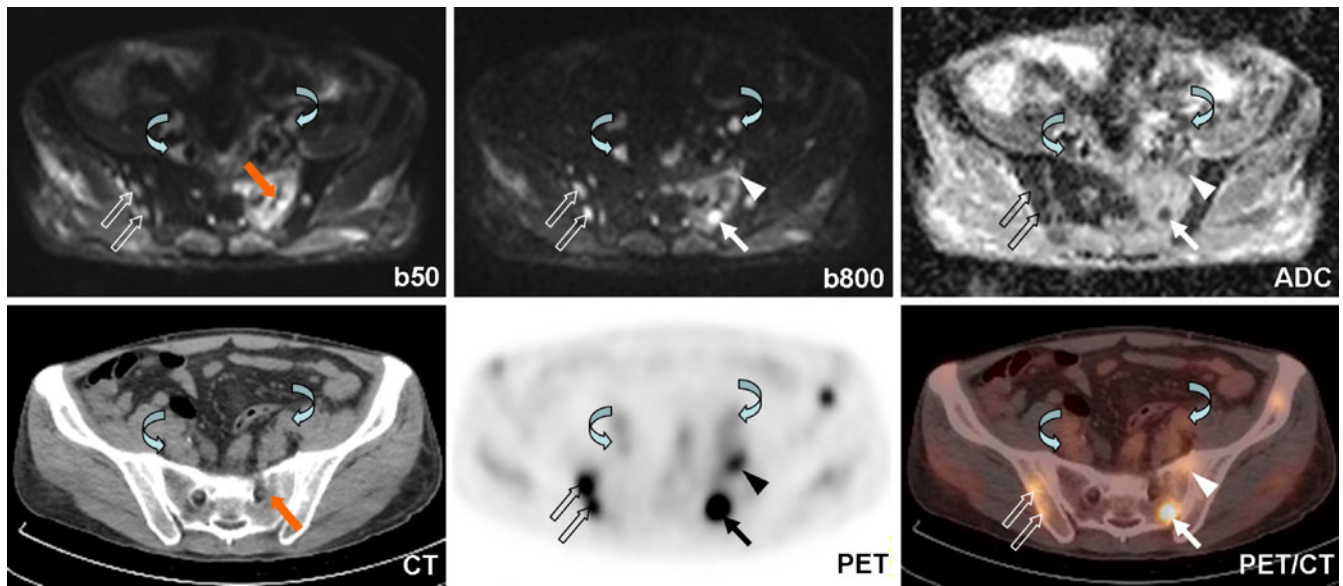


**Fig. 5** Bone marrow involvement in a 57-year-old patient (same patient as in Fig. 4) shown on DW (upper row) and PET/CT (lower row) images at about the same level. The focal lesion (arrow in white/black) over the left sacral ala stands out on the *b800* DW image, while it was masked by the surrounding high signal on the *b50* DW image. On the ADC map, this lesion shows restricted diffusion, along with another focal lesion (arrowhead), corroborating the PET/CT findings. The background left sacral ala shows a signal drop between *b50* and *b800* DW images and no restricted diffusion on the ADC map. Bone marrow oedema related to insufficiency

fracture (orange arrow) was noted, with no abnormal FDG uptake on PET. Right iliac bone focal lesions (open arrows) and involved bilateral common iliac lymph nodes (curved arrows) were also detected. Note that the focal FDG uptake of the anterior left iliac bone on PET/CT and the focal signal abnormality of the posterior left iliac bone on DW images were both depicted by the other imaging technique on adjacent slices. The signal abnormality of gluteal muscles on DW images, showing no restricted diffusion on the ADC map and faint FDG uptake, was considered inflammatory in nature

reality of the entire lymph node or focal lesion in organs [41, 42]. The size criterion for lymph node involvement (longest transverse diameter > 10 mm) was chosen on the basis of IWG criteria [1]. Instead of performing lesion detection on DW images with high *b* values ( $\geq 800$  s/mm<sup>2</sup>) [16, 19, 24], so-called diffusion-weighted whole-body imaging with background signal suppression (DWIBS), we aimed to measure the ADC of nodes identified on *b50* DW images based on this criterion. We did not perform ADC measurement on nodes smaller than 10 mm, as we chose a slice thickness of 5 mm to adapt this criterion. In addition, we did not perform MPR or MIP for image interpretation. It is said that axial source images should always be consulted since subtle lesions may be obscured in reconstructed images [19]. A recent study showed that ADC measurement provided added value in the detection of subcentimetric cervical node metastases in patients with head and neck cancers [43]. However, these authors used shortest transverse diameters. During staging, the clinical significance of involved subcentimetric lymph nodes is less important in DLBCL patients, who have larger masses and require systemic chemotherapy, whereas patients with head and neck cancers require local treatment. In future, better spatial resolution of DW images should ensure more reliable ADC analysis, and this could be useful for characterising subcentimetric nodes. The consensus reading for DWI image

analysis was a limitation since it did not allow evaluation of interobserver agreement. Finally, there is still room for technical optimisation. In the past decade, standard DW EPI sequences used a twice-refocused spin-echo bipolar diffusion scheme [44]. It has the advantage of reducing spatial distortion induced by eddy currents [44]. The latest low eddy-current gradient coil design opened the field for the usage of the monopolar scheme [18], which allows a shorter TE and therefore decreases susceptibility artefacts, increases both the signal-to-noise ratio of DW images and the accuracy of ADC measurement. Concatenation gated on respiratory cycles (i.e. separate acquisition of odd and even slices) would ensure a longer longitudinal recovery and avoid crosstalk without the need for an interslice gap.

In conclusion, whole-body DWI with ADC mapping can potentially be used for lesion detection and staging in patients with DLBCL. ADC values are decreased in DLBCL lesions. This might be helpful in confirming lymphoma involvement, although larger prospective studies are needed.

**Acknowledgements** The authors thank David Young, BSc, for editorial assistance. C.L. was supported by the Association pour la Recherche sur le Cancer. A.V., who assisted in the protocol design, was an employee of Siemens Healthcare. The other authors had full control over the data and the information submitted for publication.

## References

- Cheson BD, Horning SJ, Coiffier B et al (1999) Report of an international workshop to standardize response criteria for non-Hodgkin's lymphomas. NCI Sponsored International Working Group. *J Clin Oncol* 17:1244–1253
- Kwee TC, Kwee RM, Nievelstein RA (2008) Imaging in staging of malignant lymphoma: a systematic review. *Blood* 111:504–516
- Moog F, Bangerter M, Diederichs CG et al (1997) Lymphoma: role of whole-body 2-deoxy-2-[F-18]fluoro-D-glucose (FDG) PET in nodal staging. *Radiology* 203:795–800
- Moog F, Bangerter M, Diederichs CG et al (1998) Extranodal malignant lymphoma: detection with FDG PET versus CT. *Radiology* 206:475–481
- Schaefer NG, Hany TF, Taverna C et al (2004) Non-Hodgkin lymphoma and Hodgkin disease: coregistered FDG PET and CT at staging and restaging—do we need contrast-enhanced CT? *Radiology* 232:823–829
- Cheson BD, Pfistner B, Juweid ME et al (2007) Revised response criteria for malignant lymphoma. *J Clin Oncol* 25:579–586
- Juweid ME, Stroobants S, Hoekstra OS et al (2007) Use of positron emission tomography for response assessment of lymphoma: consensus of the Imaging Subcommittee of International Harmonization Project in Lymphoma. *J Clin Oncol* 25:571–578
- Schoder H, Noy A, Gonen M et al (2005) Intensity of 18fluorodeoxyglucose uptake in positron emission tomography distinguishes between indolent and aggressive non-Hodgkin's lymphoma. *J Clin Oncol* 23:4643–4651
- Hutchings M, Loft A, Hansen M et al (2006) FDG-PET after two cycles of chemotherapy predicts treatment failure and progression-free survival in Hodgkin lymphoma. *Blood* 107:52–59
- Lin C, Itti E, Haioun C et al (2007) Early 18F-FDG PET for prediction of prognosis in patients with diffuse large B-cell lymphoma: SUV-based assessment versus visual analysis. *J Nucl Med* 48:1626–1632
- Itti E, Lin C, Dupuis J et al (2009) Prognostic value of interim 18F-FDG PET in patients with diffuse large B-cell lymphoma: SUV-based assessment at four cycles of chemotherapy. *J Nucl Med* 50:527–533
- Sumi M, Ichikawa Y, Nakamura T (2007) Diagnostic ability of apparent diffusion coefficients for lymphomas and carcinomas in the pharynx. *Eur Radiol* 17:2631–2637
- Nakayama T, Yoshimitsu K, Irie H et al (2004) Usefulness of the calculated apparent diffusion coefficient value in the differential diagnosis of retroperitoneal masses. *J Magn Reson Imaging* 20:735–742
- King AD, Ahuja AT, Yeung DK et al (2007) Malignant cervical lymphadenopathy: diagnostic accuracy of diffusion-weighted MR imaging. *Radiology* 245:806–813
- Toh CH, Castillo M, Wong AM et al (2008) Primary cerebral lymphoma and glioblastoma multiforme: differences in diffusion characteristics evaluated with diffusion tensor imaging. *AJNR Am J Neuroradiol* 29:471–475
- Takahara T, Imai Y, Yamashita T et al (2004) Diffusion weighted whole body imaging with background body signal suppression (DWIBS): technical improvement using free breathing, STIR and high resolution 3D display. *Radiat Med* 22:275–282
- Thoeny HC, De Keyser F (2007) Extracranial applications of diffusion-weighted magnetic resonance imaging. *Eur Radiol* 17:1385–1393
- Koh DM, Collins DJ (2007) Diffusion-weighted MRI in the body: applications and challenges in oncology. *AJR Am J Roentgenol* 188:1622–1635
- Kwee TC, Takahara T, Ochiai R et al (2008) Diffusion-weighted whole-body imaging with background body signal suppression (DWIBS): features and potential applications in oncology. *Eur Radiol* 18:1937–1952
- Padhani AR, Liu G, Koh DM et al (2009) Diffusion-weighted magnetic resonance imaging as a cancer biomarker: consensus and recommendations. *Neoplasia* (New York, NY) 11:102–125
- Lichy MP, Aschoff P, Plathow C et al (2007) Tumor detection by diffusion-weighted MRI and ADC-mapping—initial clinical experiences in comparison to PET-CT. *Invest Radiol* 42:605–613
- Li S, Xue HD, Li J et al (2008) Application of whole body diffusion weighted MR imaging for diagnosis and staging of malignant lymphoma. *Chin Med Sci J* 23:138–144
- Stecco A, Romano G, Negru M et al (2009) Whole-body diffusion-weighted magnetic resonance imaging in the staging of oncological patients: comparison with positron emission tomography computed tomography (PET-CT) in a pilot study. *Radiol Med* 114:1–17
- Kwee TC, Quarles van Ufford HM, Beek FJ et al (2009) Whole-body MRI, including diffusion-weighted imaging, for the initial staging of malignant lymphoma: comparison to computed tomography. *Invest Radiol* 44:683–690
- Rahmouni A, Luciani A, Itti E (2005) Quantitative CT analysis for assessing response in lymphoma (Cheson's criteria). *Cancer Imaging* 5(Spec No A): S102–S106
- Picardi M, Soricelli A, Pane F et al (2009) Contrast-enhanced harmonic compound US of the spleen to increase staging accuracy in patients with Hodgkin lymphoma: a prospective study. *Radiology* 251:574–582
- Koh DM, Takahara T, Imai Y et al (2007) Practical aspects of assessing tumors using clinical diffusion-weighted imaging in the body. *Magn Reson Med* 6:211–224
- Nguyen TD, de Rochefort L, Spincemille P et al (2008) Effective motion-sensitizing magnetization preparation for black blood magnetic resonance imaging of the heart. *J Magn Reson Imaging* 28:1092–1100
- Uto T, Takehara Y, Nakamura Y et al (2009) Higher sensitivity and specificity for diffusion-weighted imaging of malignant lung lesions without apparent diffusion coefficient quantification. *Radiology* 252:247–254
- Bernstein MA, King KF, Zhou ZJ (2004) Handbook of MRI pulse sequences. Elsevier Academic Press, Amsterdam
- Luciani A, Vignaud A, Cavet M et al (2008) Liver cirrhosis: intravoxel incoherent motion MR imaging—pilot study. *Radiology* 249:891–899
- Kato H, Kanematsu M, Tanaka O et al (2009) Head and neck squamous cell carcinoma: usefulness of diffusion-weighted MR imaging in the prediction of a neoadjuvant therapeutic effect. *Eur Radiol* 19:103–109
- Rini JN, Leonidas JC, Tomas MB et al (2003) 18F-FDG PET versus CT for evaluating the spleen during initial staging of lymphoma. *J Nucl Med* 44:1072–1074
- de Jong PA, van Ufford HM, Baarslag HJ et al (2009) CT and 18F-FDG PET for noninvasive detection of splenic involvement in patients with malignant lymphoma. *AJR Am J Roentgenol* 192:745–753

35. Landis JR, Koch GG (1977) The measurement of observer agreement for categorical data. *Biometrics* 33:159–174
36. Mori T, Nomori H, Ikeda K et al (2008) Diffusion-weighted magnetic resonance imaging for diagnosing malignant pulmonary nodules/masses: comparison with positron emission tomography. *J Thorac Oncol* 3:358–364
37. Ho KC, Lin G, Wang JJ et al (2009) Correlation of apparent diffusion coefficients measured by 3T diffusion-weighted MRI and SUV from FDG PET/CT in primary cervical cancer. *Eur J Nucl Med Mol Imaging* 36:200–208
38. Komori T, Narabayashi I, Matsumura K et al (2007) 2-[Fluorine-18]-fluoro-2-deoxy-D-glucose positron emission tomography/computed tomography versus whole-body diffusion-weighted MRI for detection of malignant lesions: initial experience. *Ann Nucl Med* 21:209–215
39. Kwee TC, Takahara T, Koh DM et al (2008) Comparison and reproducibility of ADC measurements in breathhold, respiratory triggered, and free-breathing diffusion-weighted MR imaging of the liver. *J Magn Reson Imaging* 28:1141–1148
40. Wang J, Takashima S, Takayama F et al (2001) Head and neck lesions: characterization with diffusion-weighted echo-planar MR imaging. *Radiology* 220:621–630
41. Pileri SA, Dirnhofer S, Went P et al (2002) Diffuse large B-cell lymphoma: one or more entities? Present controversies and possible tools for its subclassification. *Histopathology* 41:482–509
42. Hunt KE, Reichard KK (2008) Diffuse large B-cell lymphoma. *Arch Pathol Lab Med* 132:118–124
43. Vandecaveye V, De Keyzer F, Vander Poorten V et al (2009) Head and neck squamous cell carcinoma: value of diffusion-weighted MR imaging for nodal staging. *Radiology* 251:134–146
44. Reese TG, Heid O, Weisskoff RM et al (2003) Reduction of eddy-current-induced distortion in diffusion MRI using a twice-refocused spin echo. *Magn Reson Med* 49:177–182
45. A predictive model for aggressive non-Hodgkin's lymphoma. The International Non-Hodgkin's Lymphoma Prognostic Factors Project. *N Engl J Med* 329:987–994